IJRCS

International Journal of Robotics and Control Systems
Vol. 6, No. 1, 2026, pp. 262-284
ISSN 2775-2658
http://pubs2.ascee.org/index.php/ijrcs

ASCEE

Modeling, Simulation, Multiobjective Optimization and Mechatronic Design of Wheel-Terrain Parameters for Better Tractability of an Autonomous Vehicle by Force Balancing Method

Mahesh Kumar Isher [a,1,*], Ramchandra Sapkota [a,2], Sanjeev Maharjan [a,3]

[a] Department of Mechanical and Aerospace Engineering, Institute of Engineering, Lalitpur, Nepal
[1] mahesh.isher@pcampus.edu.np; [2] rc.sapkota1@gmail.com; [3] mechsanjeev@ioe.edu.np
[*] Corresponding Author

ARTICLE INFO

Article History
Received July 19, 2025
Revised October 26, 2025
Accepted January 27, 2026

Keywords
Autonomous Vehicle;
Force Distribution;
Stability;
Multi-Objective Optimization;
Mechatronic Design

ABSTRACT

Stability analysis is a crucial aspect of autonomous off-road vehicle research, particularly in unknown environments. This study introduces a method for evaluating and predicting vehicle stability, based on the hypothesis that maximum stability and minimal tip-over risk are achieved when the total contact forces on the left and right wheels are equal. This condition is typically observed when roll and pitch angles are zero. The research validates this concept by analyzing orthogonal contact forces at the wheel-terrain interface, derived from the overall force distribution across the vehicle body.A sinusoidal terrain model considered as rough and uneven terrain is employed, and a multi-objective optimization problem is formulated and solved in MATLAB to minimize the difference between the left and right side contact force amplitudes. Simulation results indicate that the vehicle's tip-over tendency can be minimized by equalizing the total forces on both sides using variable force distributions by using control system.

1. Introduction

The current robotic missions to planets demonstrate the great importance of off-road autonomous vehicles for space exploration projects [1], [2]. An inhospitable environment has been monitored and to get effective remote operation, it is necessary to consider efficient locomotion systems, capable of working in uneven and rough terrain, specifically without tipover and deadlocks [3]. The mobility criteria relations such as ground clearance, orientation, traction etc. are taken into consideration for optimization [4], [5]. Also, M. P. Mann et al. proposed the range of acceptable velocities and accelerations that satisfy dynamic constraints such that the vehicle will not slide, tipover, or lose contact with the ground [6], [7]. The general formulation of an optimization problem is presented and an optimal but computationally efficient solution is proposed. An algorithm that controls the robot posture, based on the velocity model, is described [8], [9]. In this paper, a new concept based on orthogonal forces is taken into consideration in two sets of forces for the stability measure. The basic idea is to achieve a balance between the forces acting at the left and right sides of the vehicle by minimizing the difference as much as possible close to zero. This concept assumes that the difference

will be zero at zero roll and pitch angles; which is taken as the condition for minimum tip-over tendency or maximum stability.

The force balancing methods used in the terramechanics model with soil parameters are explained in [10]–[12]. Also, the force balnce approch is explained in Wiberg's PhD thesis for heavy machines for rough and deformable terrain [13]. Shear force parameters as balancing of vehicle used for lunar explorations are considered to optimize by Zou at el. [14]. Vehicle actuation forces as tipover stability considered by Aoshima et al. [15]. Some studies consider the trajectory of the bucket and the force actuated on it for the soil and a kinematically controlled bucket geometry [16]–[19]. Stability guarantee for motion planning of autonomous vehicles by motion and tractive force in simulation environment by Zhang et al. [20]. Hegazy and Sandu; Taheri et al., and Peiret et al. extended the research for steady-state predictions and dynamic simulations by integrating kinematic constraints in the calculation of the contact forces with force balance principles [21]–[23]. Deep Collision with random and greedy approach govern the environment with suitable time interval operating on different terrain structures have been illustrated [24]. 3D mapping and 3D geometry considered as vehicle tip-over prevention using gain-scheduled State-dependent Riccati Equation–based anti-rollover controller has been presented [25]. Furthermore, Tip-over detection and avoidance algorithms as stabilization strategy highlighted [26]. Patent overview based on variable CG which emphasizes reducing the turning radius of the vehicles and thereby increasing the efficiency of the vehicles [27]. Vepa includes in his book, kinematics of multi-body systems to control space vehicles in detail which ensures probabilistic representation of uncertain motion using particles and Monte Carlo integration used to control the vehicle for unknown region [28]. Mapping sensors and state-of-the art vision-based control introduced [29]. Sliding mode-based guidance strategy is proposed for the control of an autonomous vehicle collected measurement guidance strategy introduced to propel vehicle on rough terrain [30]. High-assurance controller (HAC) to tolerate concurrent software and physical failures introduced by Mao et al. [31]. The Lyapunov- Krasovski approach of the physical constraints of the steering system and direct yaw moment control employed [32]. Longitudinal slip of front wheels and sliding mode control, an integrated longitudinal and lateral control system used for wet terrain [33]. Adaptive sliding mode control of sliding-based switching non-linear vehicle model introduced [34]. A robust controller proposed for safe execution of the trajectory in the presence of state noise and dynamic model uncertainty [35]. A security-by-design framework principle for smart and complex autonomous systems proposed by Chattopadhyay et al. [36]. Multiple physical systems including skid-steer and tracked robots with real-time on-board computation using noisy sensor data on rocks and boulders, steep slopes, negative obstacles like cliffs and holes, and narrow passages were major concern of the work [37]. A variety of path planning approaches for autonomous vehicles, path planning algorithms with ultimate goal is to create a way, explore, and exploit its further values proposed by Ming et al. [38]. Dual modes for optimal mobility under different surface-traction conditions proposed the robot is capable of yaw axis mobility using differential drives with payload balances [39]. Tan et al. proposed an analysis presented based on Zero Moment Point (ZMP) concept to gain equilibrium condition without tipping over [40]. A methodology and trajectory planning of a serial manipulator using septic and nonic functions presented to prevent wear and tear with stability in weight balance way [41]. Ability of the robot to effectively navigate in rough terrain mechanism for improving maneuverability, longitudinal or lateral stability, and rollover prevention are considered with recent researches [42]. Considering the forces acting on a wheel slip reduction is defined as the reference signal specifically lateral force balance method employed [43]. Different working environments are modeled by backstepping method and hence the skew-symmetry property is validated to be feasible for nonholonomic mechanical systems [44]. Ranjan Vepa discusses kinematics of multi-body systems, and then to conservation principles in dynamics by the application of MATLAB [45]. More robust and reliable navigation strategies are reviewed with the fusion of advanced sensors and state-of-the-art control algorithms [46].

In order to achieve better stability during stirring, He Xu et al. [47] propose a trade-off design for a reconfigurable autonomous vehicle based on multi-objective optimization with respect to terramechanics. There is no single solution for the real problem, in spite of the fact that a set of solutions can be achieved, which shows that there are no best solutions considering all the objectives at a time [48]. These types of trade-off solutions derived from multi-objective optimization have already been considered for different aspects of autonomous vehicles and other vehicles [49], [50], [51]. Furthermore, an algorithm is advised to find a set of Pareto-optimal solutions to coordinate two autonomous polygonal autonomous vehicles on a plain [50]. Autonomous vehicles subject to skidding and slipping effects on the wheels are modeled at the level of kinematics and dynamics [52]. Li et al. presented stability margin measurement, which is sensitive to topheaveness and is applicable to the dynamic systems subject to inertial loads and external forces [53]. A novel approach for optimal path planning over deformable terrain of complex operating condition for maximum stability with robustness and optimality [54]. Multiobjective optimization is used in vehicle Soccer to plan the optimal path to the ball, minimize elapsed time, and maximize shot accuracy criteria [51] [55]. This work tries to optimize the stability of a vehicle by minimizing tip-over tendency based on the difference between total right-hand-side and left-hand-side forces acting on the body of the vehicle. A multi-objective optimization problem for minimum force difference is formulated and solved in MATLAB using a genetic algorithm.

The findings of this research can contribute to real-world autonomous navigation systems by helping to avoid or quickly rectify tip-over tendencies caused by rough and uneven terrain. Future work involving multidirectional force detection and decision-making control system design will build upon and emphasize the contributions of the present work.

2. Kinematic Analysis

2.1. General Introduction of the Autonomous Vehicle

This research is based on a five-wheeled mobile robot represented by the Pro-Engineer model and real robot (Fig. 1), which has four powered wheels and a 5^{th} wheel for slip estimation.

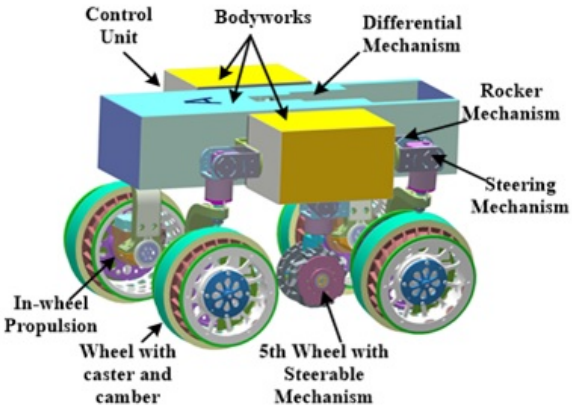

Fig. 1. Pro/E Model of WMR

The robot consists of eight sections: reconfigurable chassis (bodyworks), differential mechanism, control unit, wheels, wheel propulsion unit, 5^{th} wheel mechanism, steering mechanism and rocker mechanism.

Camera mast, GPS antenna and other scientific instruments embedded in autonomous vehicle for position variation monitoring and reconfigurable chassis facilities for proper adjustment of center of

gravity. Wheels are adjustable with two pivots at the rocker mechanism such that those can be adjusted with required camber and caster angles. The 5^{th} wheel with a steerable mechanism is employed to get the measurement of the slipping rate which is one of the major parameters to control the vehicle in rough terrain suggested by [56].

2.2. Kinematics Model of the Autonomous Vehicle

A 3-dimensional body can be rotated about three orthogonal axes, as shown in Fig. 2. Borrowing aviation terminology, these rotations will be called roll(ϕ), pitch(θ) and yaw(ψ). The basic transformation can be obtained by evaluating the corresponding angle rotation in each direction in terms of yaw, pitch and roll angles. These are explained stepwise according to basic rotation rules. Where Yaw is interpreted as the counterclockwise rotation of α around the z-axis. The rotation matrix is given by;

$$\psi = R_z(\alpha) = \begin{bmatrix} \cos\alpha & -\sin\alpha & 0 \\ \sin\alpha & \cos\alpha & 0 \\ 0 & 0 & 1 \end{bmatrix} \tag{1}$$

Note that the upper left entries of $R_z(\alpha)$ form a 2D rotation applied to the x and y coordinates, whereas the z coordinate remains constant.

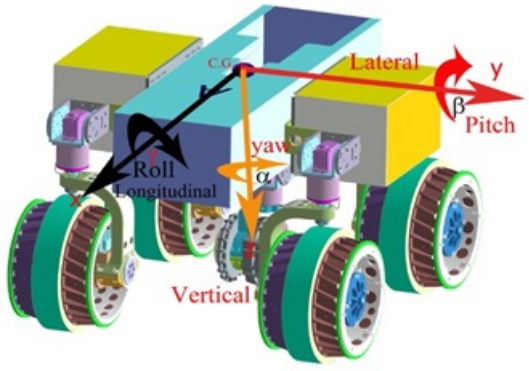

Fig. 2. SAE vehicle axis system

A pitch is a counterclockwise rotation of β about the y-axis. The rotation matrix is given by;

$$\theta = R_y(\beta) = \begin{bmatrix} \cos\beta & 0 & \sin\beta \\ 0 & 1 & 0 \\ -\sin\beta & 0 & \cos\beta \end{bmatrix} \tag{2}$$

A roll is a counterclockwise rotation of γ about the x-axis. The rotation matrix is given by;

$$\phi = R_x(\gamma) = \begin{bmatrix} 1 & 0 & 0 \\ 0 & \cos\gamma & -\sin y \\ 0 & \sin\gamma & \cos\gamma \end{bmatrix} \tag{3}$$

Two-dimensional rotation matrixes have been obtained in extended form. For illustration, the yaw matrix $R_z(\alpha)$, essentially performs a 2D rotation with respect to the x and y coordinates while z-coordinate remains unchanged. Thus, the third row and third column of $R_z(\alpha)$ seems like part of the identity matrix, while the upper right portion of $R_z(\alpha)$ seems like the two-dimensional rotation matrix. This type of rotation allows the robot to rotate on a particular axis through a particular rotational angle. By multiplying the yaw, pitch, and roll, a single rotation matrix can be formed as;

$$R(\alpha,\beta,\gamma) = R_z(\alpha)R_y(\beta)R_y(\gamma) = \begin{bmatrix} \cos\alpha\cos\beta & \cos\alpha\sin\beta\sin\gamma - \sin\alpha\cos\gamma & \cos\alpha\sin\beta\cos\gamma + \sin\alpha\sin\gamma \\ \sin\alpha\cos\beta & \sin\alpha\sin\beta\sin\gamma + \cos\alpha\cos\gamma & \sin\alpha\sin\beta\cos\gamma - \cos\alpha\sin\gamma \\ -\sin\beta & \cos\beta\sin\gamma & \cos\beta\cos\gamma \end{bmatrix} \tag{4}$$

Note that the order of rotation matrix as $R(\alpha,\beta,\gamma)$ performs the roll first, then the pitch, and finally the yaw. If the order of these operations is changed, a different rotation matrix would result. The homogeneous transformation matrix for 3D bodies can be expressed as in the 2D case; a homogeneous transformation matrix can be defined. For the 3D case, a 4X4 matrix is obtained that performs the rotation given by$R(\alpha,\beta,\gamma)$, followed by a translation (T) given by x_t, y_t, z_t. The result is;

$$T = \begin{bmatrix} \cos\alpha\cos\beta & \cos\alpha\sin\beta\sin\gamma - \sin cx\cos\gamma & \cos\alpha\sin\beta\cos\gamma + \sin cz\sin\gamma & \pi_2 \\ \sin\alpha\cos\beta & \cos\alpha\sin\beta\sin\gamma - \sin c^2\cos\gamma & \sin\alpha\sin\beta\cos\gamma - \cos c^2\sin\gamma & y_2 \\ -\sin\beta & \cos\beta\sin\gamma & \cos\beta\cos\gamma & z_2 \\ 0 & 0 & 0 & 1 \end{bmatrix} \tag{5}$$

The required motion must be satisfied before one can design a machine. Both translational and rotational motions must be analyzed in terms of position, velocity, and acceleration, which requires kinematics analysis. Dynamic analysis is required to size the links, joints, bearings, gearboxes, and actuators (motors).

The Jacobian algorithms converge locally, often producing weird end effector and platform trajectories with Jacobian inverse kinematics algorithms for autonomous vehicles. We use the existing theory of Newton algorithms to improve the quality of convergence of the Jacobian algorithms in this research.

Some assumptions are made to develop the kinematics model. Firstly, there is no deformation of wheels as well as terrain surface; secondly, the wheels of the vehicle are simplified to wafers; and thirdly wheels and surface keep point contact. The definition and description of frames are described as; Fig. 4 shows the coordinate frames of the autonomous vehicle. Then, the left front wheel means wheel 1; the left rear wheel means wheel 2; the right front wheel means wheel 3; right rear wheel means wheel 4; the meanings of coordinate frames are: G is the terrain frame, R is the reference frame of the vehicle body, D is the middle point frame of differential mechanism, T is the middle point frame of the axis of differential mechanism, $U_i(i = 1,2,3,4)$is frame fixed on the ends of left and right rockers according to the wheel number, $V_i(i = 1,2,3,4)$ is the steering frame of each wheel, $W_i(i = 1,2,3,4)$ is the wheel frame of wheel 1,2,3 and 4 respectively; R,D,T,V_i and W_i are frames at time t. $\bar{R},\bar{D},\bar{T},\bar{V}_i$ and $\bar{W}_i$ are frames at time $t-\Delta t$, besides, they are instantaneously coincidence with R,D,T,V_i and W_i respectively.

$$I = T_{W_1,C}(\delta_i) = \begin{bmatrix} \cos\delta_i & 0 & \sin\delta_i & -r\sin\delta_i \\ 0 & 1 & 0 & 0 \\ -\sin\delta_i & 0 & \cos\delta_i & -r\cos\delta_i \\ 0 & 0 & 0 & 1 \end{bmatrix} \tag{6}$$

The frame parameters are listed as d_1 is the vertical offset between vehicle reference frame R to differential frame D; d_2 is the forward offset between vehicle reference frame R to differential frame D; d_3 equal to 165 mm and is the distance between D and rocker; d_4 equal to 161.5 mm and is the distance between the middle point of rocker and frame H; d_5 equal to 178.1 mm and is distance between rocker arm and the center of the wheel; d_6 equal to forward offset between vehicle reference frame R to fifth wheel arm frame T; Other specification of the autonomous vehicle is given in Table 2. For wheel rotation by angle δ_i ; then transformation can be written as; For slipping rates by ζ_i and η_i, the transformation I given by;

$$T_{C_1,G} = \begin{bmatrix} \cos\zeta_i & \sin\zeta_i & 0 & r\theta_i + \xi_i \\ \sin\zeta_i & \cos\zeta_i & 0 & \eta_i \\ 0 & 0 & 1 & 0 \\ 0 & 0 & 0 & 1 \end{bmatrix} \tag{7}$$

The pose of reference point in terrain frame G is illustrated as a vector $U = \left[XYZ\phi_x\phi_y\phi_z\right]^T$, where, $[XYZ]^T$ and $\left[\phi_x\phi_y\phi_z\right]^T$ is the orientation vector.

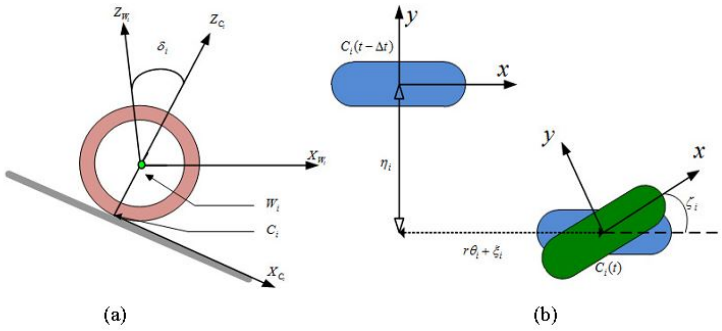

Fig. 3. (a) Rotation on contact frame (b) Incremental rotation by rolling and slip

The lower-case quantities concern the instantaneous vehicle frame R. If left and right side rocker angles $\rho$is measured by encoders then joint angles are represented by a vector as; $q = [\rho\psi_1\psi_2\psi_3\psi_4]^T$, the range of ρ and the steer angles ψ_i is $-90^0 \le \rho \le 90^0; -45^0 \le \tau \le 45^0; -90^0 \le \psi_i \le 90^\circ$. In addition, every wheel is driven independently, and its angular rotation θ_i is measured by an encoder. Jacobian matrix and motion equation is computed as;

$$\left[\dot{x}\dot{y}\dot{z}\dot{\phi}_x\dot{\phi}_y\dot{\phi}_z\right]^T = J_i\left[\dot{q}\dot{\theta}_i\dot{\varepsilon}_i\dot{\theta}_i\right]^T \tag{8}$$

Written for short as;

$$\dot{u} = J_i\dot{p} \tag{9}$$

Which gives the vehicle configuration-rate vector $\dot{d}$ in terms of the joint angular-rate vector $\dot{q}$, wheel-rolling rate $\dot{\theta}_i$, contact-angle rate $\dot{\delta}_i$, and the slip rate vector $\dot{\varepsilon}_i$. The schematic diagram of WMR and transformation coordinates is shown in Fig. 4 and the transformation graph in Fig. 6. Referring to the transformation graph of Fig. 6, the resulting equation of motion for wheel-1 is as follows: in which,

$$\begin{bmatrix}\dot{x}\\ \dot{y}\\ \dot{z}\\ \dot{\phi}_x\\ \dot{\phi}_y\\ \dot{\phi}_z\end{bmatrix} = \begin{bmatrix} J_{x,1} & J_{x,\psi} & J_{x,\theta} & J_{x,\xi} & J_{x,\zeta} & J_{x,\eta} & J_{x,\delta}\\ 0 & J_{y,\psi} & J_{y,\theta} & J_{y,\xi} & J_{y,\zeta} & J_{y,\eta} & J_{y,\delta}\\ J_{z,1} & J_{z,\psi} & J_{z,\theta} & J_{z,\xi} & J_{z,\zeta} & J_{z,\eta} & J_{z,\delta}\\ 0 & J_{\phi x,\psi} & 0 & 0 & J_{\phi k,\zeta} & 0 & J_{\phi x,\delta}\\ J_{\phi y,1} & 0 & 0 & 0 & J_{\phi y,\zeta} & 0 & J_{\phi y,\delta}\\ 0 & J_{\phi c,\psi} & 0 & 0 & J_{\phi,\zeta} & 0 & J_{\phi\varepsilon,\delta}\end{bmatrix} \times \begin{bmatrix}\dot{\rho}\\ \dot{\psi}_1\\ \dot{\theta}_1\\ \dot{\xi}_1\\ \dot{\zeta}_1\\ \dot{\eta}_1\\ \dot{\delta}_1\end{bmatrix} \tag{10}$$

In which,

$J_{x,1} = d_1$;

$J_{x,\mu} = -c\rho c\alpha_1 c\beta_1 d_3 - s\rho d_3 s\alpha_1 - c\alpha_1 d_1 s\beta_1 + s\rho c\alpha_1 d_4 s\beta_1$;

$J_{x,\theta} = c\rho rc\alpha_1 c\delta_1 c\psi_1 + rs\rho c\beta_1 c\delta_1 c\psi_1 s\alpha_1 - rs\rho c\alpha_1 c\beta_1 s\delta_1 + c\rho rs\alpha_1 s\delta_1 + rs\rho c\delta_1 s\beta_1 s\psi_1$;

$J_{x,\xi} = c\rho c\alpha_1 c\delta_1 c\psi_1 + s\rho c\beta_1 c\delta_1 c\psi_1 s\alpha_1 - s\rho c\alpha_1 c\beta_1 s\delta_1 + c\rho s\alpha_1 s\delta_1 + s\rho c\delta_1 s\beta_1 s\psi_1$;

$J_{x,\zeta} = c\rho c\alpha_1 c\beta_1 c\delta_1 d_3 + s\rho c\delta_1 d_3 s\alpha_1 + c\alpha_1 c\delta_1 d_1 s\beta_1 - s\rho c\alpha_1 c\delta_1 d_4 s\beta_1 - s\rho c\alpha_1 c\psi_1 d_3 s\delta_1 - c\rho c\beta_1 c\psi_1 d_3 s\alpha_1 s\delta_1 - s\rho c\psi_1 d_s s\beta_1 s\delta_1 + c\psi_1 d_1 s\alpha_1 s\beta_1 s\delta_1 - s\rho c\psi_1 d_4 s\alpha_1 s\beta_1 s\delta_1 - c\beta_1 d_1 s\delta_1 s\psi_1 + s\rho c\beta_1 d_4 s\delta_1 s\psi_1 + c\rho c\alpha_1 d_s s\delta_1 s\psi_1 + s\rho c\beta_1 d_5 s\alpha_1 s\delta_1 s\psi_1 + c\rho d_3 s\beta_1 s\delta_1 s\psi_1$;

$J_{x,\eta} = s\rho c\psi_1 s\beta_1 - c\rho c\alpha_1 s\psi_1 - s\rho c\beta_1 s\alpha_1 s\psi_1$;

$J_{x,\delta} = c\beta_1 c\psi_1 d_1 - s\rho c\beta_1 c\psi_1 d_4 - c\rho c\alpha_1 c\psi_1 d_5 - s\rho c\beta_1 c\psi_1 d_5 s\alpha_1 - c\rho c\psi_1 d_3 s\beta_1 - s\rho c\alpha_1 d_3 s\psi_1 + c\rho c\beta_1 d_3 s\alpha_1 s\psi_1 - s\rho d_5 s\beta_1 s\psi_1 + k_1 s\alpha_1 s\beta_1 s\psi_1 - s\rho d_4 s\alpha_1 s\beta_1 s\psi_1$

Where, 'c' stands for cosine and 's' for sine of respective angles. Also, $\dot{\xi}_1, \dot{\eta}_1$ and $\dot{\zeta}_1$ are rolling slip rate, lateral slip rate and turn-slip rotation rate respectively. Similar equations are derived for other wheels, wheel 2, 3, 4 and 5 , which give the particular wheel motion and the connecting joints rotation to the vehicle body motion. The net vehicle motion is the combined effect of wheels and is obtained by combining all wheel motion equation all

together into a single matrix equation as:

$$\begin{bmatrix} I_6 \\ I_6 \\ I_6 \\ I_6 \\ I_6 \\ I_6 \\ I_6 \end{bmatrix} \begin{bmatrix} \dot{x} \\ \dot{y} \\ \dot{z} \\ \dot{\phi}_x \\ \dot{\phi}_y \\ \dot{\phi}_x \end{bmatrix} = J \begin{bmatrix} \dot{q} \\ \dot{\theta} \\ \dot{\varepsilon} \\ \dot{\delta} \end{bmatrix} \tag{11}$$

Where, J is formed by each wheel Jacobian J. Besides this, J represents a sparse matrix. These transformations and the Jacobian matrix are used for simulation to determine wheel positions.

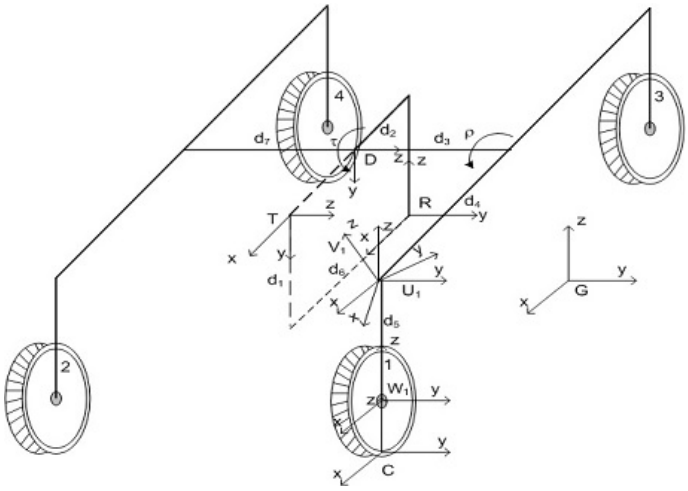

Fig. 4. Schematic diagram of WMR and transformation coordinate system

3. Force Distribution

3.1. Force Analysis of the Autonomous Vehicle

Regarding Newtonian dynamics, internal and external forces are considered for system analysis. For example, external forces can be a contact force, such as the traction force at the contact point of a driving wheel, or a body force, such as the gravitational force on the vehicle's body. The basic forces acting upon a vehicle at the point of contact between the wheel and terrain are shown in Fig. 5.

Considering four wheels of the vehicle and three forces in three directions on each wheel as shown in Fig. 4, hence the forces along x, y and z directions of the local coordinate system are considered for the analysis. These are the force components along x, y and z directions at the point of contact of each wheel. So, for wheel i ; T_i = Tractive force along x-direction at the point of contact of wheel i, L_i = Lateral force along y direction at the point of contact of wheel i and N_i = Normal force along z-direction at the point of contact of wheel i, where i = 1, 2, 3 and 4. 5^{th} wheel is not considered for analysis because it lies in the central axis of the vehicle and is not taken as a contributor to unbalanced forces.

For the first case, to analyze force distribution along x-direction, all wheels are separated as right-hand side and left-hand side forces. Therefore, each side could be resolved into a single resultant set of forces as follows:
Right-hand side forces(F_r),

$$F_r = \sum_{i=1}^{n_j} F_{x_j} \tag{12}$$

and left-hand side forces(F_l),

$$F_l = \sum_{i=1}^{n_l} F_{x_j} \tag{13}$$

F_r, F_l are the forces on the right-hand side and left-hand side respectively. F_x is the force along x direction on ith wheel. n_r, n_l are the number of wheels on the right-hand side and left-hand side respectively.

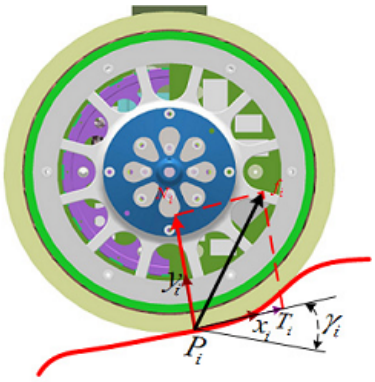

Fig. 5. Wheel-ground interface on uneven terrain

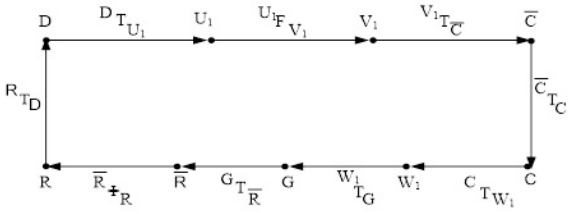

Fig. 6. Transformation graph

3.2. Condition for Maximum Stability

The basic concept is to balance the forces acting at the left and right sides of the vehicle by minimizing the difference as much as possible close to zero. This concept assumes that the difference will be zero at zero roll and pitch angles; which is the condition for minimum tip-over tendency and maximum stability. This can be expressed as thus:

$$F_r - F_l \cong 0 \tag{14}$$

or,

$$\sum_{i=1}^{n_j} F_{x_i} - \sum_{i=1}^{n_i} F_{x_i} \cong 0 \tag{15}$$

For the whole vehicle's body to be stable similar analysis is carried out for y and z-directions respectively as follows:

$$\sum_{i=1}^{n_2} F_{y_n} - \sum_{i=1}^{n_i} F_{y_i} \cong 0 \tag{16}$$

$$\sum_{i=1}^{n} F_{z_i} - \sum_{i=1}^{n} F_{z_j}^{n} \cong 0 \tag{17}$$

and hence in absolute term;

$$\left|\sum_{i=1}^{n} F_r\right| - \left|\sum_{i=1}^{n} F_i\right| \cong 0 \tag{18}$$

Furthermore, the normalized three-dimensional forces (3D-forces) are considered for simplicity but in practice, it is not the exact situation, for the reason it is convenient to compute the resultant force on right-hand side and

left-hand side separately as Euclidean Vector Sum of forces. For any real number considered for resultant force in the respective direction then shown in Fig. 7;

$$|r| = |(X,Y,Z)| = \sqrt{X^2+Y^2+Z^2}\vec{r}_1 + \vec{r}_2 = \bar{R} : R = \sqrt{X^2+Y^2+Z^2} \tag{19}$$

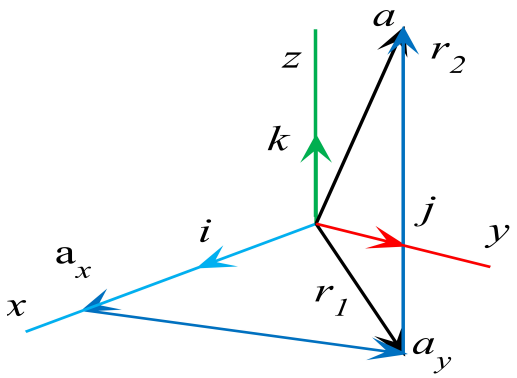

Fig. 7. Euclidean vector force representation

By this basic consideration of resultant force, the force equation in quadratic form is now introduced for analysis and also in MATLAB simulation, it is convenient and logical to consider resultant forces in the form of the quadratic equation. So, Eq. (15) can be rewritten as;

$$\sqrt{\sum_{i=1}^{n}(F_r)^2} - \sqrt{\sum_{i=1}^{n_j}(F_l)^2} \cong 0 \tag{20}$$

3.3. Formulation of Multi-Objective Optimization

Sources of forces in an autonomous vehicle available from self-weight, torque applied by actuators also unwanted and unbalanced forces are due to obstacles and inclinations. The forces of the environment such as wind blow and others are neglected.

Minimization problem formulation for the force distribution comprises as follows for all values of roll angle (α) less or equal to the maximum permissible value;

$$\min_{T_r,L_e,N_r} \left|\sum_{i=1}^{N_r} F_r\right| - \left|\sum_{i=1}^{n_i} F_i\right| \forall\alpha \le \alpha_{\max} \tag{21}$$

T_i, L_i, N_i are force components, more precisely the set of vector forces of $[T_1, L_1, N_1, T_3, L_3, N_3]$ are force vectors on right-hand side of wheels (wheel 1 and 3) while $[T_2, L_2, N_2, T_4, L_4, N_4]$ are force vectors on left-hand side of wheels (wheel 2 and 4). For the simulation in MATLAB the quadratic equation is considered as Eq. (22) based on resultant forces on the right and left-hand sides.

$$\min_{T_i,L_p,N_i} \sqrt{\sum_{i=1}^{n_r}(F_r)^2} - \sqrt{\sum_{i=1}^{n_1}(F_l)^2} \quad \forall\alpha \le \alpha_{\max} \tag{22}$$

If we elaborate on Eq. (17) with the component of forces, the expression for the minimization function is derived as follows, which is used for MATLAB simulation:

$$\min_{T_1,L_1,N_1} \left\{\sqrt{T_1^2 + {L_1}^2 + {N_1}^2} + \sqrt{T_3^2 + {L_3}^2 + {N_3}^2}\right\} \quad - \quad \left\{\sqrt{{T_2}^2 + {L_2}^2 + {N_2}^2} + \sqrt{{T_4}^2 + {L_4}^2 + {N_4}^2}\right\} \tag{23}$$

In the proposed algorithm, the left-hand forces and right-hand forces are separately calculated. In addition, the forces calculated can be correlated with instantaneous roll and pitch angles. The forces in each direction are to be summed up and the difference of these two sides' forces is computed such that the absolute values can be compared in the next step for stability measure and prediction.

Furthermore, to compute forces, the vectors $f_i = \left[f_i^x f_i^y f_i^z\right]^T, i = \{1,2,3,4\}$, represent wheel terrain interaction forces and are expressed in the inertial frame $\{XYZ\}$. The vectors $P_i = \left[p_i^x p_i^y p_i^z\right]^T, i = \{1,2,3,4\}$, are directed from the wheel-terrain contact points to the robot center of mass p_c and are expressed in the inertial frame $\{XYZ\}$ shown in Table 1.

Table 1. Algorithm to simulate genetic algorithm multi-objective optimization

Force difference minimization $\sqrt{\sum_{r=n}^{n_r}(f_r)^2} - \sqrt{\sum_{l=n}^{n_l}(f_l)^2}$	
determine objective function(OF);	1
assign number of generations to 0 (t=0)	2
randomly create individuals in initial population P(t)	3
while termination criterion is not satisfied do	4
t=t+1;	5
for each i-th individual in the population P(t) do;	6
randomly generate RHS and LHS force difference sets;	7
$for, T_i, L_i, N_i := 1_{\text{to}} T_i', L_i', N_i';$	8
for, $r := 1$ to $n_r + 1$ and $i := 1$ to $n_l + 1$; evaluate $\sqrt{\sum_{r=n}^{n_r}(f_r)^2} - \sqrt{\sum_{l=n}^{n_l}(f_l)^2}$	9
If $\sqrt{\sum_{i=1}^{n}(F_r)^2} - \sqrt{\sum_{i=1}^{n_j}(F_l)^2} \cong 0$ then	10
$\varepsilon := [\bar{\varepsilon}]$	11
$\min_{T_r, L_e, N_r} \left\lvert\sum_{i=1}^{N_r} F_r\right\rvert - \left\lvert\sum_{i=1}^{n_i} F_i\right\rvert \forall \alpha \le \alpha_{\max}$	12
End if	13
Until Termination Condition	13

The vector $f_x = \left[F_x^x F_x^y F_x^x M_x^x M_x^y M_x^z\right]^T$ at the center of mass represents mainly the effects of gravitational and inertial forces. A set of quasi-static force balance Eq. 24 for the four-wheeled vehicle is determined for the right and left sides see [57].

$$\begin{bmatrix} 1 & 0 & 0 & & 1 & 0 & 0 \\ 0 & p_1^z & p_1^y & \cdots\cdots & 0 & p_4^z & {p_4}^y \\ -p_1^z & 0 & -p_1^x & & -{p_4}^z & 0 & -{p_4}^x \\ -p_1^y & p_1^x & 0 & & -{p_4}^y & {p_4}^x & 0 \end{bmatrix} \begin{bmatrix} f_1 \\ f_2 \\ f_3 \\ f_4 \end{bmatrix} = f_s \tag{24}$$

4. Simulations and Results

4.1. Simulations

The terrain model is considered as a Sine function as given in Eq. (25) and Table 2 shows the basic specifications of the mobile robot, the data is measured after the final production of the prototype suggested by [58].

$$\mathrm{y} = 10^{*} \sin\left(\mathrm{x}^{*}\mathrm{pi}/50\right) \tag{25}$$

Table 2 shows the typical specifications of the autonomous vehicle, the data is measured after the final production of WMR on a plane ground. Fig. 8, Fig. 9, and Fig. 10 show the alignment of double sine curve terrain as a rough terrain to simulate. A particular type of terrain created by wooden blocks which contains carpet on the top surface as shown in Fig. 9 and 10.

For simulation, terrain equation is used to simulate a similar environment of terrain including kinematic transformations to run the autonomous vehicle on rough terrain [58] [59]. Here also we must ensure that autonomous vehicles do not to tipover and deadlocked. In the context of energy consumption and corresponding drawbar pull must be optimized. That means energy consumption must be minimized whereas drawbar pull must be maximized at rough terrain and minimized on flat terrain.

Table 2. The basic specifications of the wheeled mobile robot

Particulars	**Specification**
Wheel Radius (m)	0.0885
Wheel Base (m)	0.323
Wheel Stance (m)	0.33
Ground Clearance (m)	0.166 ~ 0.256
Average velocity (m/s)	0.269
Power (Watt)	Maximum 200 W
Length × Width × Height((m)	0.5×0.44×0.40
Mass (Kg)	15
d1, d2	0
d3, d7(m)	0.165
d4(m)	0.162
d5(m)	0.178
d6(m)	0

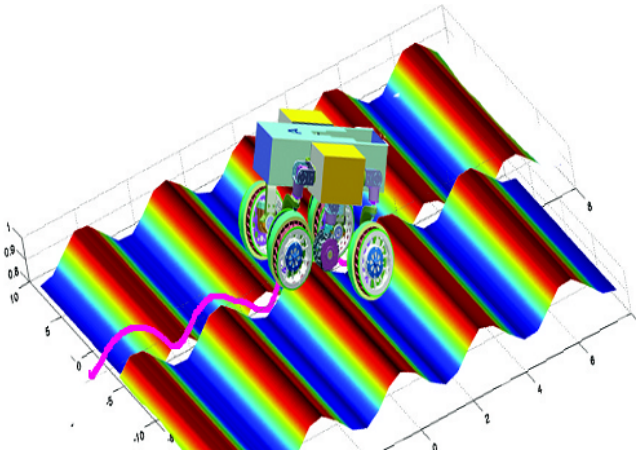

Fig. 8. Terrain used in simulation study

Fig. 9. Typical Type A rough terrain

Fig. 10. Typical Type B rough terrain

The other type like terrain with sand or gravel may be the option to test vehicles with known soil parameters such as cohesion, internal friction angle and shear deformation modulus. From Coulomb's equation for maximum shear strength τ_{max} that can withstand by ground with internal friction angle ϕ and the corresponding wheel terrain model is shown in Fig. 11 by K. Iagnemma et al. [60], [61];

$$\tau_{max} = (c + \sigma_{max} \tan \phi) \tag{26}$$

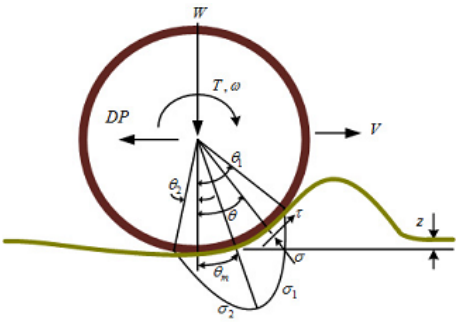

Fig. 11. Rigid wheels on deformable terrain

The known quantities are the vertical load W, torque T, angular speed of the wheel ω, wheel linear speed V and sinkage z measured with on-board sensors. Hence, the force balance equations for W, DP and T are given by;

$$W = rb\left(\int_{\theta_1}^{\theta_2} \sigma(\theta)\cos\theta \cdot d\theta + \int_{\theta_1}^{\theta_2} \tau(\theta)\sin\theta \cdot d\theta\right) \tag{27}$$

$$DP = rb\left(\int_{\theta_1}^{\theta_2} \tau(\theta)\cos\theta \cdot d\theta - \int_{\theta_1}^{\theta_2} \sigma(\theta)\sin\theta \cdot d\theta\right) \tag{28}$$

$$T = r^2 b \int_{\theta_1}^{\theta_2} \tau(\theta) \cdot d\theta \tag{29}$$

The shear stress ($\tau(\theta)$) is defined as;

$$\tau(\theta) = \left(c + \omega(\theta)\tan\phi\left(1 - e^{-\frac{r}{k}\{\theta_1 - \theta - (1-i))(\sin\theta_1 - \sin\theta)\}}\right)\right) \tag{30}$$

For a wide range of sinkage coefficients, the equations are simplified for computation as follows;

$$W = \frac{rb}{\theta_m(\theta_1 - \theta_m)} \left\{ \begin{array}{l} \sigma_m(\theta_1 \cos\theta_m - \theta_m \cos\theta_1 - \theta_1 + \theta_m) \\ +\tau_m(\theta_1 \sin\theta_m - \theta_m \sin\theta_1) \end{array} \right\} \tag{31}$$

$$DP = \frac{rb}{\theta_m(\theta_1 - \theta_m)} \left\{ \begin{array}{l} \tau_m(\theta_1 \cos\theta_m - \theta_m \cos\theta_1 - \theta_1 + \theta_2) \\ +\sigma_m(\theta_1 \sin\theta_m - \theta_2 \sin\theta_1) \end{array} \right\} \tag{32}$$

$$T = \frac{1}{2} r^2 b(\tau_m \theta_1 + c\theta_m) \tag{33}$$

Where, i, r, b, and k are wheel slip ratio, wheel radius, wheel width and shear deformation modulus respectively. Thus, wheel slip ratio, $i = 1 - (V/r\omega)$. Fitness function on the basis can be written by recalling equations (31), (32) and (33) with noise-induced on it;

$$\left\{ \begin{array}{l} P_i' = P(T_i) \\ T_i' = T_i(c + \Delta c, k + \Delta k, \phi + \Delta\phi) \\ N_i' = N_i(c + \Delta c, k + \Delta k, \phi + \Delta\phi) \end{array} \right. \tag{34}$$

Where, Δk, $\Delta\phi$ and Δc are defined as terramechanics noise intensities regarding shear deformation modulus, internal friction angle and soil cohesion. Due to changes in terrain parameters as a major concern for the effect of operational parameters, other noise sources like noise from measuring encoders, wheel terrain interaction, frictional variations etc are not taken into the record. Different Pareto solutions for the different parameters in the form of Pareto front and corresponding values are obtained in the next chapter.
The overall constraint of noise intensities is assumed as;

$$-0.1 \leq (\Delta c \text{ or } \Delta k \text{ or } \Delta\phi) \leq +0.1 \tag{35}$$

$$\forall i, i = \{1 \ldots n\}$$

The physical constraints of the vehicle such that vehicle wheels remain in contact with the terrain have been considered for optimization of wheel-terrain interaction. In terms of wheel-terrain normal forces N_i must remain positive as a constraint;

$$N_i > 0 \forall i, i = \{1 \ldots n\} \tag{36}$$

For torque produced, the limits are given by;

$$T_i^{\min} \leq (T_i \cdot r) \leq T_i^{\max} \tag{37}$$

$$\forall i, i = \{1..n\}$$

By using the Coulomb friction or force coefficient model, the approximated tractive force at the surface of contact must not exceed the maximum force that the terrain can hold up;

$$T_i \leq \mu N_i \forall i, i = \{1 \ldots n\} \tag{38}$$

Particularly, in the equations 31 to 33, the constraint of angular positions has been limited for this study as given below.

$$20^0 \leq \theta_1 \leq 40^\circ$$
$$20^\circ \leq \theta_2 \leq 40^\circ$$
$$0^\circ \leq \theta_m \leq 20^\circ$$

4.2. Results

In Table 3 basic parameters considered for the simulation work have been illustrated for optimization.The graph showing wheel odometry distance versus force experienced on each wheel is presented in Fig. 12, Fig. 13 and Fig. 14. Here, the force distributions in the three directions are presented separately.

Fig. 16 shows the proposed method's control system design. The tracking performance of the proposed algorithm is evaluated through the average root mean square errors with respect to variables through sensors. The effectiveness of the proposed method is tested and verified by simulation results. Fig. 17 demonstrates the empirical values of the Cumulative Distribution Function (CDF) of power drawn at differed noise levels in the solution region. Fig. 18 shows the respective CDF of drawbar pull at different noise levels and Fig. 19 shows the CDF for a normal load. Which indicates the variation range of forces acting upon the vehicle for different parameters.

Table 3. Parameter setting

Parameters	Settings
Chromosome	15 bits per decision variable with Binary coding
Population	Pop. size 100; for Archive (or sec. pop. 100)
Selection	Binary tournament selection
Crossover operator	Uniform crossover
Crossover rate	0.8
Mutation rate	$\frac{1}{\text{chromosomelength}}$ for ZDT1, ZDT4 and ZDT6; $\frac{1}{\text{bitnumberpervariable}}$ for FON and KUR
Mutation operator	Bit-flip mutation
Ranking scheme	Pareto ranking
Diversity operator	Niche count with radius 0.01 in the normalized objective space.
Evaluation number	50000

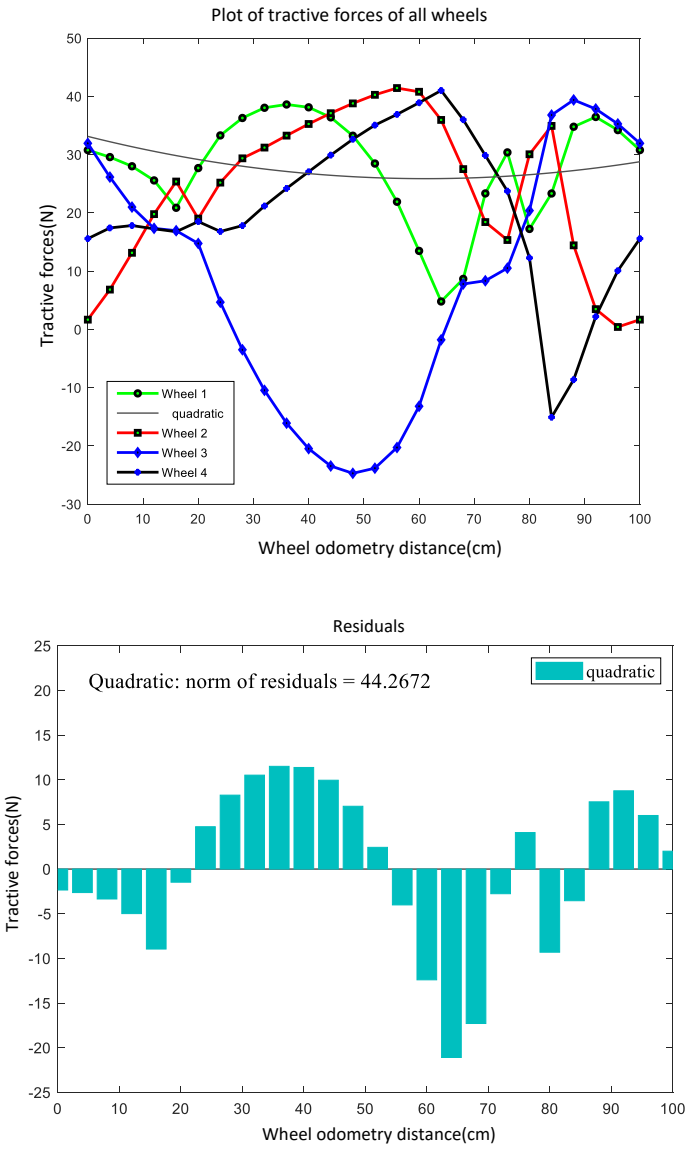

Fig. 12. Plot of wheel odometry distance vs. tractive forces of all wheels and residuals

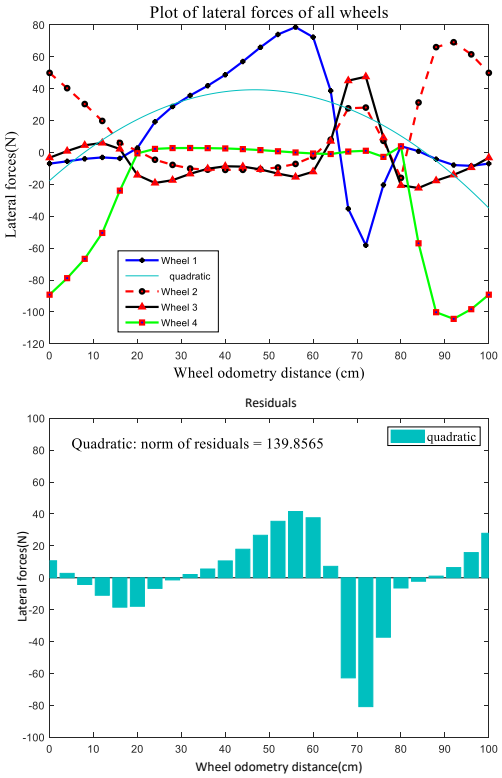

Fig. 13. Plot of wheel odometry distance vs. lateral forces of all wheels

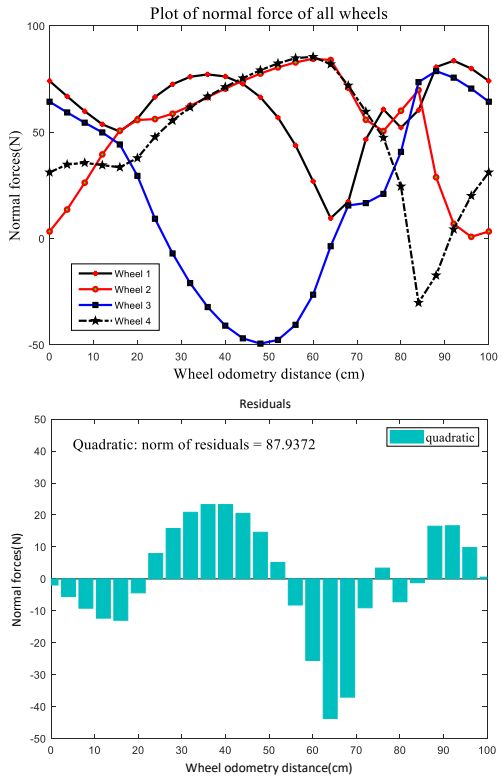

Fig. 14. Plot of wheel odometry distance vs. normal forces of all wheels

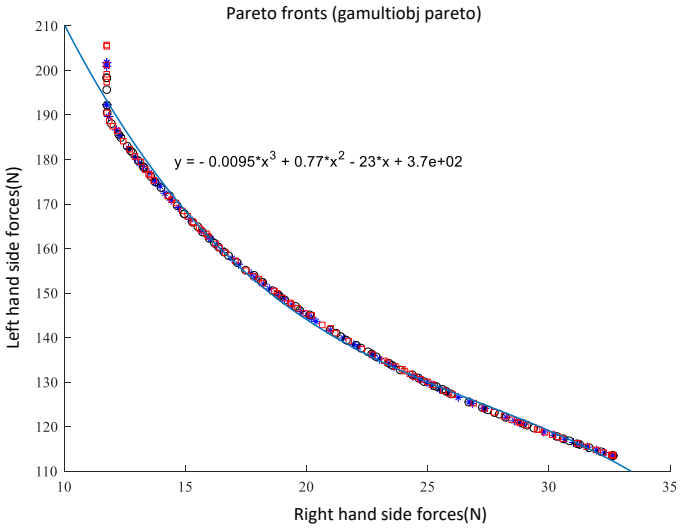

Fig. 15. The non-dominated Pareto front between right-hand side and left-hand side forces

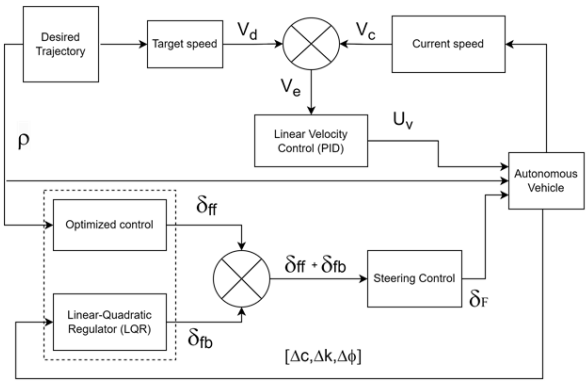

Fig. 16. Control system design

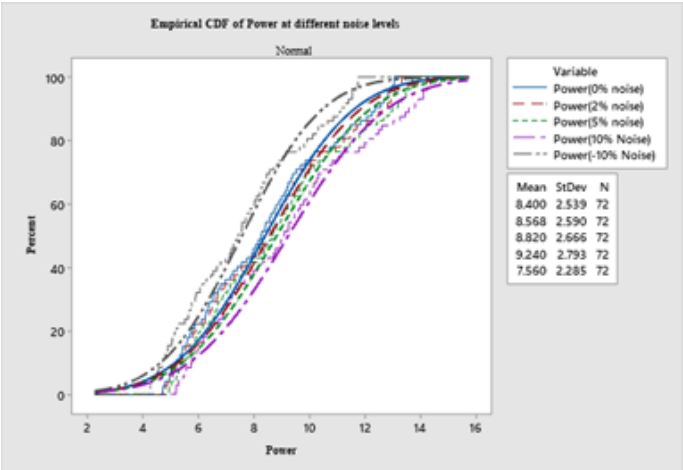

Fig. 17. Empirical Cumulative Distribution Function (CDF) of power at different noise levels

4.3. Mechatronic Design

A conceptual diagram of robust motion control system design is presented in Fig. 20 which is used to design a system to optimize tractive force and respective power consumption. A bottleneck in developing algorithms for enabling autonomous-driving capabilities is the amount of testing and verification of the different components contained in Fig. 21 which includes an overview of the basic architecture for the control system. The main contribution is to reduce the tracking and lateral errors of the autonomous vehicle, especially while going through obstacles, by developing a hybrid longitudinal and lateral control system. The longitudinal control design is based on the geometrical curvature information and is integrated with the PID controller for speed control purposes.

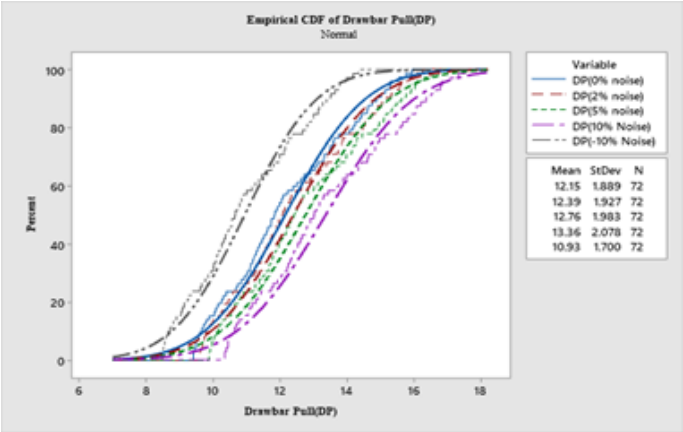

Fig. 18. Empirical Cumulative Distribution Function(CDF) of drawbar pull at different noise levels

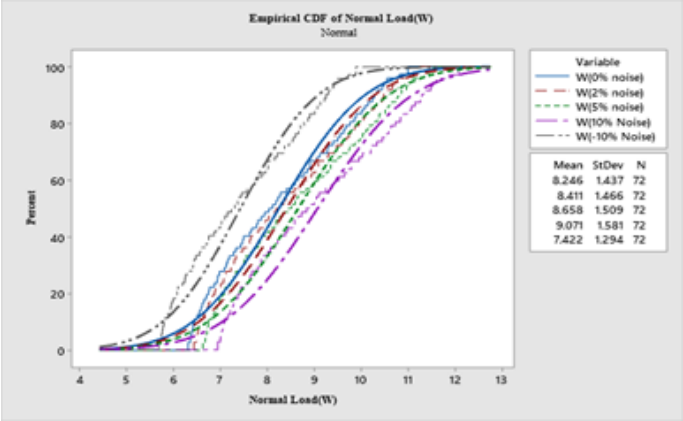

Fig. 19. Empirical Cumulative Distribution Function (CDF) of normal load at different noise levels

The desired speed of the vehicle is generated from the vehicle's current speed and curvature profile of the terrain. Furthermore, the feedforward optimal set of solution control is applied to solve lateral errors of the trajectory by controlling the steering movement decision mode of the vehicle, especially caused by highly rough and deformable terrain. The Linear Quadratic Regulator (LQR) will be applied to decrease the errors caused by environmental and external disturbances. The control system design of the proposed method is shown in Fig. 22. The tracking performance of the proposed algorithm is evaluated through the average root mean square errors with respect to variables through sensors. The effectiveness of the proposed method is tested and verified by simulation results.

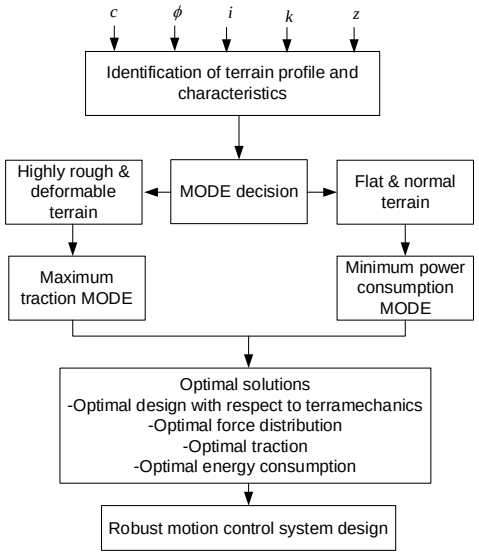

Fig. 20. Conceptual diagram of robust motion control system design

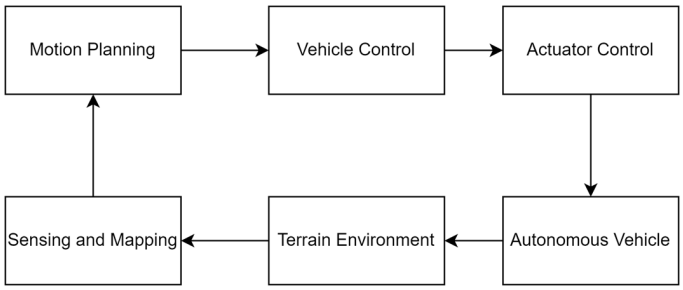

Fig. 21. Basic Architecture for control system

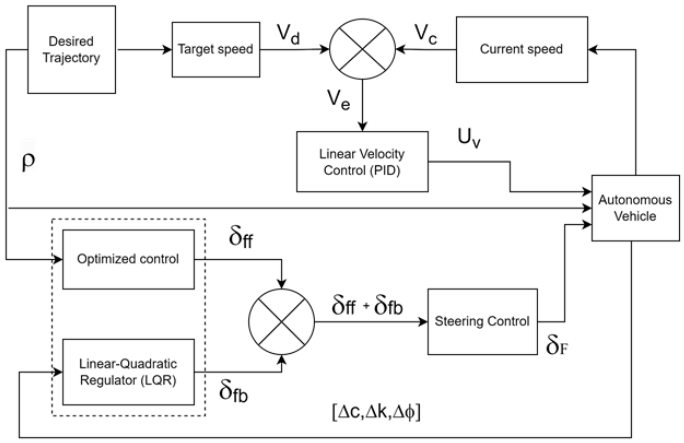

Fig. 22. Control system design

5. Conclusion and Future Work

5.1. Conclusion

The size of the residuals in force curves, obtained by plugging the computed solution back into the original equations, differs by several orders of magnitude. In a three-dimensional force environment along the x, y and

z directions, namely the tractive force, the lateral force and the normal force are separately analyzed and from the graph, it is clear that the robot is balanced within the constraint value with nominal force variations.

The residual plot shows the residuals on the vertical axis whereas on the horizontal axis, the independent variable is plotted. Around the horizontal axis, the residual plots are randomly dispersed with a linear regression model appropriate for the data; otherwise, a non-linear model is more appropriate.

A residual as sensitivity analysis is the distance of a point from the curve and is positive when the point is above the curve, and is negative when the point is below the curve. The difference of Normal Residual, which gives the average sum of the plots of the forces on the right and left sides, is estimated as the difference in the residuals = 44.2708 – 27.8388 = 16.4320.

As this study considers symmetric design of vehicle has its center of gravity lies in the center of the body, so force imbalance greater than 50 percent on either side greatly influence the stability and tip-over tendency. Grand et al. [8] illustrated in terms of angular movement less than 50^0 applied for tipover stability. If we consider 100% stable as the ideal case, that is when the difference of these two resultant forces equals zero; then it is concluded that the vehicle is 37.1170161% unstable and 62.8829838% stable. The non-dominated Pareto front obtained between two sides forces that are taken as conflicting objectives are plotted using gamultiobj solver for multi-objective optimization as shown in Fig. 15. The Pareto front obtained with the following parameter values associated with the analysis as an initial guess of 0.1 for all variables with a population size of 60, Pareto Fraction of 70% and evaluated with the upper bound and lower bound of [5,5] and $[-5,-5]$ respectively. Solutions obtained here in the Pareto front are non-dominated to each other.

However, variation in forces on one side will affect the resultant force on the other side. The change in initial guesses as the global optimal solution is quite sensitive to such variable perturbation in its vicinity; the implementation solution may result in a different set of objective values than that of the theoretical optimal solution. It is seen that with the same guesses, Pareto front changes with different trade-off solutions. Hence, the Cumulative Distribution Function (CDF) of the drawbar pull, power and normal load verifies the force fluctuation within the range to operate the vehicle without abnormal tilt. The Linear-Quadratic Regulator (LQR) control system regulates the variations with inputs in changes in terrain parameters Δc, Δk and $\Delta\phi$.

5.2. Future Work

The designer must emphasize that finding robust solutions less sensitive to variable perturbations in their neighborhoods can be taken as future work. Such solutions can be used to control the vehicle more accurately in terms of force distribution as a parameter that is correlated with the maximum permissible threshold by indirect measurement of permissible(safe) roll and pitch angle so that the vehicle does not tip over and deadlock.

Author Contribution: All authors contributed equally to the main contributor to this paper. All authors read and approved the final paper.

Funding: This research was funded by University Grants Commission- Nepal, grant number "PhD-74/75-Engg-03".

Acknowledgment: The authors wish to thank Institute of Engineering, Department of Mechanical and Aerospace Engineering and University Grant Commission of Nepal. This work was supported in part by a grant from University Grant Commission of Nepal.

Conflicts of Interest: The authors declare no conflict of interest.The funders had no role in the design of the study; in the collection, analyses, or interpretation of data; in the writing of the manuscript, or in the decision to publish the results.

References

[1] S. Farritor, H. Hacot, and S. Dubowsky, "Physics-based planning for planetary exploration," in *Proceedings. 1998 IEEE International Conference on Robotics and Automation*, vol. 1, pp. 278–283, 1998, https://doi.org/10.1109/ROBOT.1998.676399.

[2] F. Islam, M. Nabi, and J. E. Ball, "Off-road detection analysis for autonomous ground vehicles: A review," *Sensors*, vol. 22, no. 21, p. 8463, 2022, https://doi.org/10.3390/s22218463.

[3] J. Manero Álvarez, "Design and development of a ugv (unmanned ground vehicle) for rescue applications," *Universitat Politècnica de Catalunya*, 2024, https://hdl.handle.net/2117/410384.

[4] G. Freitas, G. Gleizer, F. Lizarralde, and L. Hsu, "Multi-objective optimization for kinematic reconfiguration of mobile robots," in *2010 IEEE International Conference on Automation Science and Engineering*, pp. 686–691, 2010, https://doi.org/10.1109/COASE.2010.5584545.

[5] L. Wang, Y. Qi, B. He, and Y. Xu, "An efficient autonomous exploration framework for autonomous vehicles in uneven off-road environments," *Drones*, vol. 9, no. 7, p. 490, 2025, https://doi.org/10.3390/drones9070490.

[6] M. P. Mann and Z. Shiller, "Dynamic stability of a rocker bogie vehicle: Longitudinal motion," in *Proceedings of the 2005 IEEE international conference on robotics and automation*, pp. 861–866, 2005,https://doi.org/10.1109/ROBOT.2005.1570225.

[7] T. Czapla and M. Pawlak, "Simulation of the wheel-surface interaction dynamics for all-terrain vehicles," *Applied Mechanics*, vol. 3, no. 2, pp. 360–374, 2022, https://doi.org/10.3390/applmech3020022.

[8] C. Grand, F. Benamar, F. Plumet, and P. Bidaud, "Stability and traction optimization of a reconfigurable wheel-legged robot," *The International Journal of Robotics Research*, vol. 23, no. 10-11, pp. 1041–1058, 2004, https://doi.org/10.1177/0278364904047616.

[9] Z. Jian, Z. Yan, X. Lei, Z. Lu, B. Lan, X. Wang, and B. Liang, "Dynamic control barrier function-based model predictive control to safety-critical obstacle-avoidance of mobile robot," *arXiv*, 2022, https://doi.org/10.1109/icra48891.2023.10160857.

[10] E. Karpman, J. Kövecses, and M. Teichmann, "Terramechanics models augmented by machine learning representations," *Journal of Terramechanics*, vol. 107, pp. 75–89, 2023, https://doi.org/10.1016/j.jterra.2023.03.002.

[11] E. Wallin and M. Servin, "Data-driven model order reduction for granular media," *Computational Particle Mechanics*, vol. 9, no. 1, pp. 15–28, 2022, https://doi.org/10.1007/s40571-020-00387-6.

[12] E. Wallin, V. Wiberg, F. Vesterlund, J. Holmgren, H. Persson, and M. Servin, "Learning multiobjective rough terrain traversability," *arXiv*, 2022, https://doi.org/10.1016/j.jterra.2022.04.002.

[13] V. Wiberg, *Terrain machine learning*, PhD thesis, Umeå University, 2023, https://books.google.com.np/books?id=JLj2zwEACAAJ.

[14] M. Zou, L. Xue, H. Gai, Z. Dang, S. Wang, and P. Xu, "Identification of the shear parameters for lunar regolith based on a ga-bp neural network," *Journal of Terramechanics*, vol. 89, pp. 21–29, 2020, https://doi.org/10.1016/j.jterra.2020.02.003.

[15] K. Aoshima and M. Servin, "Examining the simulation-to-reality gap of a wheel loader digging in deformable terrain," *Multibody system dynamics*, vol. 64, no. 1, pp. 121–148, 2025, https://doi.org/10.48550/arXiv.2310.05765.

[16] D. Eriksson and R. Ghabcheloo, "Comparison of machine learning methods for automatic bucket filling: An imitation learning approach," *Automation in Construction*, vol. 150, p. 104843, 2023, https://doi.org/10.1016/j.autcon.2023.104843.

[17] B. Frank, J. Kleinert, and R. Filla, "Optimal control of wheel loader actuators in gravel applications," *Automation in Construction*, vol. 91, pp. 1–14, 2018, https://doi.org/10.1016/j.autcon.2018.03.005.

[18] Y. Meng, H. Fang, G. Liang, Q. Gu, and L. Liu, "Bucket trajectory optimization under the automatic scooping of lhd," *Energies*, vol. 12, no. 20, p. 3919, 2019, https://doi.org/10.3390/en12203919.

[19] S. Wang, Y. Yin, Y. Wu, and L. Hou, "Modeling and verification of an acquisition strategy for wheel loader's working trajectories and resistance," *Sensors*, vol. 22, no. 16, p. 5993, 2022, https://doi.org/10.3390/s22165993.

[20] L. Zhang, R. Zhang, T. Wu, R. Weng, M. Han, and Y. Zhao, "Safe reinforcement learning with stability guarantee for motion planning of autonomous vehicles," *IEEE transactions on neural networks and learning systems*, vol. 32, no. 12, pp. 5435–5444, 2021, https://doi.org/10.1109/TNNLS.2021.3084685.

[21] S. Hegazy and C. Sandu, "Experimental investigation of vehicle mobility using a novel wheel mobility number," *Journal of Terramechanics*, vol. 50, no. 5-6, pp. 303–310, 2013, https://doi.org/10.1016/j.jterra.2013.09.005.

[22] S. Taheri, C. Sandu, S. Taheri, E. Pinto, and D. Gorsich, "A technical survey on terramechanics models for tire–terrain interaction used in modeling and simulation of wheeled vehicles," *Journal of Terramechanics*, vol. 57, pp. 1–22, 2015, https://doi.org/10.1016/j.jterra.2014.08.003.

[23] A. Peiret, E. Karpman, L. L. Kovács, J. Kövecses, D. Holz, and M. Teichmann, "Modelling of off-road wheeled vehicles for real-time dynamic simulation," *Journal of Terramechanics*, vol. 97, pp. 45–58, 2021, https://doi.org/10.1016/j.jterra.2021.04.001.

[24] C. Lu, Y. Shi, H. Zhang, M. Zhang, T. Wang, T. Yue, and S. Ali, "Learning configurations of operating environment of autonomous vehicles to maximize their collisions," *IEEE Transactions on Software Engineering*, vol. 49, no. 1, pp. 384–402, 2022, https://doi.org/10.1109/TSE.2022.3150788.

[25] H. M. Nair and C. Sujatha, "Vehicle tip-over prevention using gain-scheduled state-dependent riccati equation–based anti-rollover controller," *Proceedings of the Institution of Mechanical Engineers, Part D: Journal of Automobile Engineering*, vol. 235, no. 2-3, pp. 807–828, 2021, https://doi.org/10.1177/0954407020948317.

[26] A. Toledo Fuentes, F. Kempf, M. Kipfmüller, T. Bergmann, and M. J. Prieto, "Tip-over detection and avoidance algorithms as stabilization strategy for small-footprint and lightweight mobile manipulators," *Machines*, vol. 11, no. 1, p. 44, 2022, https://doi.org/10.3390/machines11010044.

[27] A. Berdiev, G. Bahadirov, D. Zhang, W. Xuelin, and L. Qian, "Analysis of the design of lifting and transporting vehicles with a variable center of gravity–a literature and patent overview," *International Journal of Engineering Trends and Technology*, vol. 69, pp. 56–65, 2021, https://doi.org/10.14445/22315381/IJETT-V69I12P208.

[28] R. Vepa, *Dynamics and control of autonomous space vehicles and robotics*, Cambridge University Press, 2019, https://doi.org/10.1017/9781108525404.

[29] A. Bajcsy, S. Bansal, E. Bronstein, V. Tolani, and C. J. Tomlin, "An efficient reachability-based framework for provably safe autonomous navigation in unknown environments," in *2019 IEEE 58th Conference on Decision and Control*, pp. 1758–1765, 2019, http://doi.org/10.1109/CDC40024.2019.9030133.

[30] C. Mellucci, P. P. Menon, C. Edwards, and P. G. Challenor, "Environmental feature exploration with a single autonomous vehicle," *IEEE Transactions on Control Systems Technology*, vol. 28, no. 4, pp. 1349–1362, 2019, http://doi.org/10.1109/TCST.2019.2908141.

[31] Y. Mao, Y. Gu, N. Hovakimyan, L. Sha, and P. Voulgaris, "S$\mathcal{L}_1$1-simplex: safe velocity regulation of self-driving vehicles in dynamic and unforeseen environments," *ACM Transactions on Cyber-Physical Systems*, vol. 7, no. 1, pp. 1–24, 2023, https://doi.org/10.1145/3564273.

[32] G. Cai, L. Xu, Y. Liu, J. Feng, J. Liang, Y. Lu, and G. Yin, "Robust preview path tracking control of autonomous vehicles under time-varying system delays and saturation," *IEEE Transactions on Vehicular Technology*, vol. 72, no. 7, pp. 8486–8499, 2023, https://doi.org/10.1109/TVT.2023.3250328.

[33] A. Norouzi, A. Barari, and H. Adibi-Asl, "Stability control of an autonomous vehicle in overtaking manoeuvre using wheel slip control," *International Journal of Intelligent Transportation Systems Research*, vol. 18, no. 2, pp. 320–330, 2020, https://doi.org/10.1007/s13177-019-00200-6.

[34] A. Norouzi, R. Kazemi, and S. Azadi, "Vehicle lateral control in the presence of uncertainty for lane change maneuver using adaptive sliding mode control with fuzzy boundary layer," *Proceedings of the Institution of Mechanical Engineers*, vol. 232, no. 1, pp. 12–28, 2018, https://doi.org/10.1177/0959651817733222.

[35] S. Khaitan, Q. Lin, and J. M. Dolan, "Safe planning and control under uncertainty for self-driving," *IEEE Transactions on Vehicular Technology*, vol. 70, no. 10, pp. 9826–9837, 2021, https://doi.org/10.1109/TVT.2021.3108525.

[36] A. Chattopadhyay, K.-Y. Lam, and Y. Tavva, "Autonomous vehicle: Security by design," *IEEE Transactions on Intelligent Transportation Systems*, vol. 22, no. 11, pp. 7015–7029, 2020, https://doi.org/10.1109/TITS.2020.3000797.

[37] R. Thakker, N. Alatur, D. D. Fan, J. Tordesillas, M. Paton, K. Otsu, O. Toupet, and A.-a. Agha-mohammadi, "Autonomous off-road navigation over extreme terrains with perceptually-challenging conditions," in *International Symposium on Experimental Robotics*, pp. 161–173, Springer, 2020, https://doi.org/10.1007/978-3-030-71151-1_15.

[38] Y. Ming, Y. Li, Z. Zhang, and W. Yan, "A survey of path planning algorithms for autonomous vehicles," *SAE international journal of commercial vehicles*, vol. 14, no. 1, pp. 97–109, 2021, https://doi.org/10.4271/02-14-01-0007.

[39] P. Ben-Tzvi and W. Saab, "A hybrid tracked-wheeled multi-directional mobile robot," *Journal of Mechanisms and Robotics*, vol. 11, no. 4, p. 041008, 2019, https://doi.org/10.1115/1.4043599.

[40] H. Tan, R. Muntashir, L. Nurahmi, B. Pramujati, A. Kurniawan, U. Wasiwitono, and S. Caro, "Stability analysis of a reconfigurable and mobile cable-driven parallel robot," *IEEE Access*, vol. 12, pp. 14182–14193, 2024, https://doi.org/10.1109/ACCESS.2024.3355134.

[41] P. A. Parikh, R. Trivedi, and J. Dave, "Trajectory planning for the five degree of freedom feeding robot using septic and nonic functions," *International Journal of Mechanical Engineering and Robotics Research*, vol. 9, no. 7, pp. 1043–1050, 2020, https://doi.org/10.18178/ijmerr.9.7.1043-1050.

[42] T. S. A. Attia, "Design and development of a novel reconfigurable wheeled robot for off-road applications," *Virginia Polytechnic Institute and State University*, 2018, https://www.researchgate.net/profile/Tamer-Attia-3/publication/337339078_Design_and_Development_of_a_Novel_Reconfigurable_Wheeled_Robot_for_Off-Road_Applications/links/5dd3b765a6fdcc7e138d41f8/Design-and-Development-of-a-Novel-Reconfigurable-Wheeled-Robot-for-Off-Road-Applications.pdf.

[43] T. Zielinska and W. Ge, "Slip reduction method dedicated for autonomous wheeled platforms," *International Journal of Mechatronics and Automation*, vol. 7, no. 4, pp. 201–211, 2020, https://doi.org/10.1504/IJMA.2020.110859.

[44] T. Zou, J. Angeles, and F. Hassani, "Dynamic modeling and trajectory tracking control of unmanned tracked vehicles," *Robotics and Autonomous Systems*, vol. 110, pp. 102–111, 2018, https://doi.org/10.1016/j.robot.2018.09.008.

[45] R. Vepa, *Dynamics and control of autonomous space vehicles and robotics*, Cambridge University Press, 2019, https://books.google.co.id/books?id=k5SODwAAQBAJ&hl=id&source=gbs_navlinks_s.

[46] K. Borkar *et al*., "Stability analysis and navigational techniques of wheeled mobile robot: A review, processes," *Processes*, vol. 11, no. 12, p. 3302, 2023, https://doi.org/10.3390/pr11123302.

[47] H. Xu, D. Tan, Z. Zhang, Z. Gao, G. Peng, and C. Li, "Trade-offs design of mobile robot based on multi-objective optimization with respect to terramechanics," in *2009 IEEE/ASME International Conference on Advanced Intelligent Mechatronics*, pp. 239–244, 2009, https://doi.org/10.1109/AIM.2009.5230007.

[48] K. Deb, "Multi-objective optimisation using evolutionary algorithms: an introduction," in *Multi-objective evolutionary optimisation for product design and manufacturing*, pp. 3–34, 2011, https://doi.org/10.1007/978-0-85729-652-8_1.

[49] H. Zhang, "Multi-objective simulation-optimization for earthmoving operations," *Automation in construction*, vol. 18, no. 1, pp. 79–86, 2008, https://doi.org/10.1016/j.autcon.2008.05.002.

[50] H. Chitsaz, J. M. O'Kane, and S. M. LaValle, "Exact pareto-optimal coordination of two translating polygonal robots on an acyclic roadmap," in *IEEE International Conference on Robotics and Automation*, vol. 4, pp. 3981–3986, 2004, https://doi.org/10.1109/ROBOT.2004.1308892.

[51] J.-H. Kim, Y.-H. Kim, S.-H. Choi, and I.-W. Park, "Evolutionary multi-objective optimization in robot soccer system for education," *IEEE Computational Intelligence Magazine*, vol. 4, no. 1, pp. 31–41, 2009, https://doi.org/10.1109/MCI.2008.930985.

[52] K. Alipour, A. B. Robat, and B. Tarvirdizadeh, "Dynamics modeling and sliding mode control of tractor-trailer wheeled mobile robots subject to wheels slip," *Mechanism and Machine Theory*, vol. 138, pp. 16–37, 2019, https://doi.org/10.1016/j.mechmachtheory.2019.03.038.

[53] X. Li, L. Wu, Q. Sun, and T. Song, "Online dynamic tip-over analysis for a wheeled mobile dual-arm robot with an improved tip-over moment stability criterion," *Journal of Robotics*, vol. 2021, 2021, https://doi.org/10.1155/2021/9913335.

[54] H. Taghavifar, S. Rakheja, and G. Reina, "A novel optimal path-planning and following algorithm for wheeled robots on deformable terrains," *Journal of Terramechanics*, vol. 96, pp. 147–157, 2021, https://doi.org/10.1016/j.jterra.2020.12.001.

[55] L. R. C. Drehmer, H. M. Gomes, and W. J. Paucar Casas, "An interval-based multi-objective robust design optimization for vehicle dynamics," *Mechanics Based Design of Structures and Machines*, vol. 51, no. 12, pp. 7076–7101, 2023, https://doi.org/10.1080/15397734.2022.2088557.

[56] O. A. Ani, H. Xu, and G. Zhao, "Analysis and modeling of slip for a five-wheeled mobile robot (wmr) in an uneven terrain," in *2011 IEEE International Conference on Mechatronics and Automation*, pp. 154–159, 2011, https://doi.org/10.1109/ICMA.2011.5985648.

[57] K. D. Iagnemma and S. Dubowsky, "Terrain estimation for high-speed rough-terrain autonomous vehicle navigation," in *Unmanned Ground Vehicle Technology IV*, vol. 4715, pp. 256–266, 2002, https://doi.org/10.1117/12.474457.

[58] H. Xu, Z. Zhang, K. Alipour, K. Xue, and X. Z. Gao, "Prototypes selection by multi-objective optimal design: application to a reconfigurable robot in sandy terrain," *Industrial Robot: An International Journal*, 2011, https://doi.org/10.1108/01439911111179110.

[59] C. Min *et al.*, "Autonomous driving in unstructured environments: How far have we come?," *arXiv*, 2024, https://doi.org/10.48550/arXiv.2410.07701.

[60] K. Iagnemma, H. Shibly, and S. Dubowsky, "On-line terrain parameter estimation for planetary rovers," in *Proceedings 2002 IEEE international conference on robotics and automation (Cat. No. 02CH37292)*, vol. 3, pp. 3142–3147, 2002, https://doi.org/10.1109/ROBOT.2002.1013710.

[61] L. L. Kovács, B. Ghotbi, F. González, P. Niksirat, K. Skonieczny, and J. Kövecses, "Effect of gravity in wheel/terrain interaction models," *Journal of Field Robotics*, vol. 37, no. 5, pp. 754–767, 2020, https://doi.org/10.1002/rob.21924.